Bibliographical reference

A Diffraction Model for Acoustical Ray-Tracing Based on the Energy Flow Lines Concept, Alexis Billon and Jean-Jacques Embrechts, Acta Acustica **vol. 99** (Number 2), 2013, pp. 260-267

DOI

https://doi.org/10.3813/AAA.918608

Acta Acustica united with Acustica
Vol. 99 (2013) 260 – 267

DOI 10.3813/AAA.918608

A Diffraction Model for Acoustical Ray-Tracing Based on the Energy Flow Lines Concept

Alexis Billon, Jean-Jacques Embrechts
Intelsig research group, University of Liège, Sart-Tilman B28, B-4000 Liège, Belgium. billon.alexis@gmail.com

Summary
Geometrical acoustics models are currently the most popular prediction tools in room-acoustics due to their low computing load. However, they seldom take into account the diffraction occurring at free edges. Moreover, the existing diffraction models implemented in geometrical acoustics algorithms are either limited to specularly reflected paths or either present excessive computation load. Recently, a diffraction model based on an approximation of the far-field direction of the Poynting's vector around half-planes has been introduced for computing the scattering due to faceted dielectric objects. In this article, this model is developed to handle obliquely incident waves and is implemented within an acoustic ray-tracing software using the analogy between the Poynting's and the acoustic intensity vectors. The proposed model can handle both diffuse and specular reflections and sets no limit in terms of reflection or diffraction order. The first results obtained by ray-tracing agree well with the uniform theory of diffraction and the boundary elements method for single and double diffraction problems even if the interference effects are neglected and as long as the number of emitted rays is sufficient. Moreover, the additional computation load to handle diffraction is shown to be low compared to the one from a classical ray-tracing algorithm.

PACS no. 43.20.Dk, 43.20.El, 43.28.Js, 43.55.Br, 43.55.Ka, 43.58.Ta

1. Introduction

In geometrical acoustics, the wavelength of the sound waves is assumed to be negligible in comparison to the characteristic size of the obstacles and the phase information of the waves is usually neglected [1, 2]. One of the geometrical acoustic models is the ray-tracing algorithm that models the propagation of sound waves as rays carrying only acoustic power [1]. The ray-tracing algorithm is very popular in room-acoustics due to their relatively low computation time compared to the more computationally intensive methods solving the wave equation. Computation time is particularly important for (real-time) auralizations [3, 4] since these techniques require the calculation of room impulse responses.

However, the geometrical acoustics models are often limited due to their inability to handle edge diffraction effects [5, 6]. In fact, they assume that energy travels along straight lines (in homogeneous propagation media). To handle edge diffraction, two models based on the wave theory are particularly popular in geometrical acoustics: the uniform theory of diffraction (UTD) [7, 8] and the Biot-Tolstoy-Medwin model (BTM) [9, 10, 11].

The UTD [7, 8] is an asymptotic expansion (high frequency assumption) of the exact expression of the diffraction of a wave by a wedge of arbitrary angle and provides a continuous and bounded diffracted field.. An expression of the sound field around the edge is obtained in the frequency domain. Due to the low cost of the evaluation of the diffracted field, this model has found several applications in room acoustics [12, 13, 14, 15]. On the other hand, the BTM is an exact expression of the sound field around a finite edge in the time domain for arbitrary locations of the sound source and the receiver. It has also been applied in room acoustics [16, 17]. Compared to the UTD, the BTM leads to more accurate results, but with an increase of the computation time, even if more computationally efficient solutions have been developed [18, 19, 20, 21]. In the case of an infinite diffracting wedge, both methods give the same results [22].

One of the major problems to apply these coherent diffraction models to geometrical acoustics algorithms is the search for all the diffracted paths. If specular reflections are considered, images of the diffracting edges onto the room's surfaces can be recursively constructed [6, 16, 23] similarly to the classical source image method [24, 25]. As a consequence, the same accelerating techniques as those used in the classical source image method can be applied, such as binary space partitioning [17, 26]. However, each diffracting edge becomes a primary source in this method and the number of images to evaluate grows exponentially with the order of reflection, restricting the practical application to low reflection orders. Another method consists in the detection of propagation paths including the specular reflections and the diffracted paths,

Received 6 September 2011,
accepted 27 November 2012.

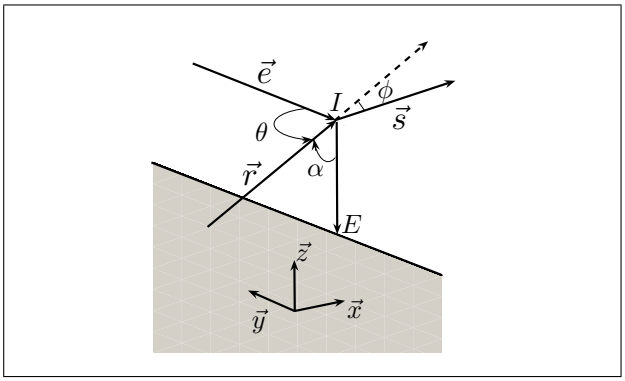

Figure 1. Plane wave incident over a half-plane. $\vec{r}$ is the incident wave vector and $\vec{s}$ the deflected one. $\vec{e}$ is the edge line direction. $\vec{IE}$ is the shortest distance between the intersection point I on the edge. In this particular example, $\vec{e}$ is collinear to $\vec{y}$ and $\vec{IE}$ to $\vec{z}$. α is the incidence angle (comprised between 0 and π) in respect to the half-plane and θ is the incidence angle (defined between 0 and $\pi/2$) in respect to the edge line. ϕ is the deflection angle of the ray into the plane expanded by $\vec{r}$ and $\vec{IE}$ and is its value is negative when directed into the shadow zone.

by tracing from the sound source beams [12, 13, 27] or frustrums [14, 15]. Once discovered, these paths, passing exactly at the edge of the diffracting wedges, are used to propagate the energy from the source to the receiver.

In all coherent methods, the diffracted paths are only associated with specular reflections. The contributions of diffuse reflections are totally neglected. On the other hand, the ray-tracing method [28, 29] can take into account diffuse reflections [1, 30, 31]. In this case, the problem is that the probability for a sound ray to intersect a diffracting edge is extremely weak (theoretically 0). The detection of the diffracting edge therefore implies the definition of virtual surfaces extending them in space such as they become visible by the propagating sound rays [32, 33, 34, 35]. So, these algorithms imply the development of incoherent, energy-based, diffraction models.

In Ref. [32], the sound rays crossing the virtual surface are then redirected randomly. This model obtains good agreement with measurements with a limited computation load but its physical basis seem dubious. The three other models [33, 34, 35] are more computationally demanding. Each ray detecting the diffracting edge results in the emission of several tens of diffracted rays according to some defined directivity patterns. In the first model [33], the energy carried by the diffracted rays is evaluated using the Keller's geometrical theory of diffraction [36] which is based on the same assumptions as the UTD. The directivity pattern is derived from the uncertainty relation for the second model [34] and from a shifted screen model for the third one [35].

Recently, Hesse and Ulanowski [37] have introduced a diffraction model based on the direction of the energy flow lines [38] behind an infinite half-plane to evaluate the light scattering created by ice crystals. In this model, the rays are deflected in the shadow zone depending on the distance between the ray and the edge, similarly to Refs. [34] and [35] . However, the rays are not split up and the number of traced rays remains constant along a simulation. The deflection angle is based on an approximation of the time-averaged Poynting's vector[39, 38] direction in the far field. For perpendicular incident waves, the analytically evaluated angular energy density was in good agreement with the one obtained from the rigorous Sommerfeld's solution [38] in the far field.

In this paper, the Hesse and Ulanowski's model is extended to oblique incidence and then implemented in an acoustic ray-tracing software in section 2. The ray-tracing results are compared to the one obtained using the UTD in section 3 with a particular emphasis on the sampling issue. The additional computation load due to the diffraction model is investigated in section 4. An application to a Y-shaped barrier, presenting a double diffraction phenomenon, is presented in section 5.

2. Energy flow lines diffraction model

2.1. Deflection angle

The problem under consideration is the diffraction of plane waves by a half-plane. Let's define θ the angle between the incoming wave vector and the diffracting edge (Figure 1),

$$\cos\theta = \frac{\vec{r}\cdot\vec{e}}{|\vec{r}|\times|\vec{e}|}, \tag{1}$$

where $\vec{r}$ is the ray direction and $\vec{e}$ the edge direction whose orientation is chosen so that $0 < \theta \leq \pi/2$. In this section, the waves propagate in a plane perpendicular to the edge. θ is then equal to $\pi/2$ and the problem has an exact solution [38, 39].

Let's now define the angle α between the incoming waves and the half-plane such as (Figure 1)

$$\cos\alpha = -\frac{\vec{r}\cdot\vec{IE}}{|\vec{r}|\times|\vec{IE}|}, \tag{2}$$

where I is the intersection point between the ray and the transparent plane including the half-plane and E the projection of I on the edge. For waves incident perpendicularly to the half-plane ($\alpha = \pi/2$), Hesse and Ulanowski [37] proposed an empirical expression of the far field deflection angle of the energy flow lines given through the direction of the time-averaged Poynting's vector [38] behind the half-plane,

$$\phi(d) = -\arctan\frac{\lambda}{4\pi^2 d}, \tag{3}$$

where $d = |\vec{IE}|$ is the distance between the passing plane wave and the diffracting edge and λ is the wavelength. This empirical relation is evaluated by matching the direction of the flow lines obtained by numerically solving the Maxwell's equation for the same problem [37]. In this problem, the edge is assumed to be infinite and that both the source and the receptor are located far enough from

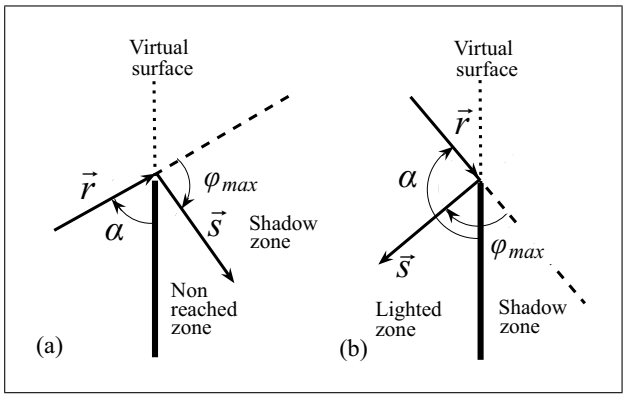

Figure 2. (a) Oblique incidence rays for $\alpha < \pi/2$ with the rays having the greater deflection angle $\phi_{max} = -\pi/2$ evaluated using equation (4). (b) Oblique incidence ray for $\alpha > \pi/2$ with the rays having the greater deflection angle $\phi_{max} = -\pi/2$ evaluated using equation (4).

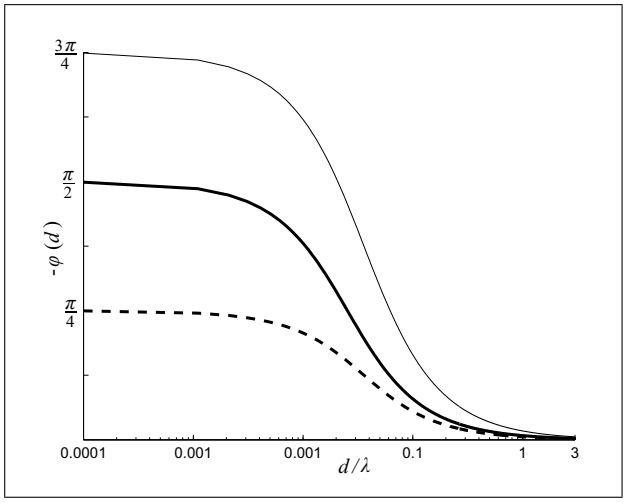

Figure 3. Evolution of the deflection angle $-\phi(d)$ obtained using equation (5) as a function of the edge-ray distance d/λ for an incidence angle $\alpha=\pi/4$ (thin line), $\pi/2$ (bold line) and $3\pi/4$ (dashed line). For $\alpha=\pi/2$ (bold line), equation (5) is equivalent to equation (3).

the half-plane. These assumptions are also made in the geometrical theory of diffraction [36] or the uniform theory of diffraction [7, 8]. In acoustics, the Poynting's vector can be interpreted as the acoustic intensity vector [40] and the link with the acoustic ray-tracing algorithm is therefore straightforward.

Equation (3) is very intuitive both in geometrical optics [38] and in acoustics [40]: the closer of the diffracting edge the rays travel, the greater their deflection angle (Figure 3 for $\alpha = \pi/2$). Moreover, a good agreement with the Sommerfeld's solution [38] can be obtained in the far field [37]. The proposed concept deals only with energetic quantity and cannot thus predict the phase jump occurring at the edge. On the other hand, the predicted field is continuous at the shadow boundary.

For oblique incident waves ($\alpha \neq \pi/2$ whereas $\theta = \pi/2$, the propagation still occurring in a plane perpendicular to the edge), the following expression can be obtained [41]:

$$\phi(d) = -\arctan\frac{\lambda}{4\pi^2 d\sin\alpha}. \quad (4)$$

However, the maximum of the deflection angle ϕ_{max} reaches $-\pi/2$ as d approaches 0 which can create some artifacts in the obtained diffracted field. If $\alpha < \pi/2$, the zone defined between $\phi = -\pi/2$ and $\alpha - \pi$ cannot be reached by the diffracted waves and the energy field in the shadow zone becomes discontinuous (Figure 2a). Similarly, if $\alpha > \pi/2$, the plane waves can be redirected in the lighted zone as if the waves were reflected by the diffracting edge (Figure 2b). So, the deflection angle must be bound by $\pi - \alpha$ and a correction factor is added to equation (4), such as

$$\phi(d) = -2\frac{\pi-\alpha}{\pi}\arctan\frac{\lambda}{4\pi^2 d\sin\alpha}. \quad (5)$$

Figure 3 presents the obtained deflection angle computed with equation (5) as function of the edge-ray distance for an incidence angle $\alpha=\pi/4$, $\pi/2$ and $3\pi/4$. It should be noted that for $\alpha=\pi/2$, equation (5) can be reduced to equation (3). For $\alpha = \pi/4$, the obtained diffraction angles cover the entirety of the shadow zone. The predicted deflected waves are thus spread on a wider angle ($\phi_{max} = -3\pi/4$) compared to the perpendicular incident configuration ($\phi_{max} = -\pi/2$). On the other hand, for $\alpha = 3\pi/4$, these deflected waves are squeezed on a narrower angle ($\phi_{max} = -\pi/4$).

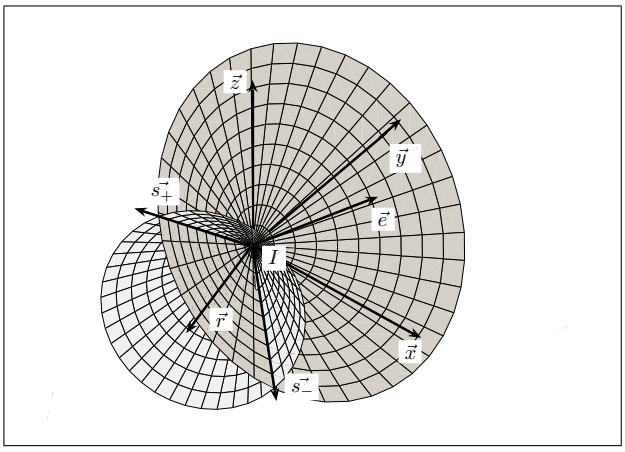

Figure 4. Notations of the diffraction cone (medium gray, apex in I, aperture 2θ and direction $\vec{e}$) and the deflection cone (light gray, apex in I, aperture 2ϕ and direction $\vec{r}$). $\vec{s_+}$ and $\vec{s_-}$ represent the two possible directions of the diffracted ray $\vec{s}$. In this particular example, θ is equal to $\pi/3$, $\phi = \pi/6$ and $\vec{e} = [1/\sqrt{2}; 0; 1/\sqrt{2}]$.

2.2. Rays in a plane oblique to the edge

When the ray lies in a plane oblique to the edge ($\theta \neq \pi/2$), the diffracted ray must propagate along the diffraction cone [36]. This cone is oriented along the edge and its aperture angle is equal to 2θ. Moreover, the diffracted ray must also lie on the deflection cone oriented along $\vec{r}$ and having a 2ϕ aperture (Figure 4). In fact, for obliquely incident rays, equation (5) define a solid angle and creates

also a cone. So, the diffracted ray direction $\vec{s}$ must satisfy the following conditions:

$$\begin{cases} \cos\phi = \frac{\vec{s}\cdot\vec{r}}{|\vec{s}|\times|\vec{r}|}, \\ \cos\theta = \frac{\vec{s}\cdot\vec{e}}{|\vec{s}|\times|\vec{e}|}, \\ |\vec{s}| = 1. \end{cases} \tag{6}$$

In the considered configuration, the intersection of these two cones having the same apex creates two lines. In the Cartesian coordinate system $\vec{e}_1, \vec{e}_2, \vec{e}_3$ linked to the diffraction cone which is oriented following the edge-line (the edge direction defining $\vec{e}_3$ in this coordinate system), the direction vectors of these lines can be evaluated by

$$\begin{aligned} S_1^{\pm} &= \pm\sqrt{1-(S_2^{\pm})^2-(S_3^{\pm})^2}, \\ S_2^{\pm} &= -\frac{\cos\phi-\cos^2\theta}{\sin\theta}, \\ S_3^{\pm} &= \cos\theta. \end{aligned} \tag{7}$$

Now, this solution must express within the coordinate system $\vec{x}, \vec{y}, \vec{z}$ in which the geometry of the problem is described in the ray-tracing algorithm (it should be noted that $\vec{x}, \vec{y}, \vec{z}$ are independent of the screen direction). So, this solution must be rotated twice following the angles ψ and ω defined depending on the edge line direction $\vec{e} = [x_e; y_e; z_e]$,

$$\begin{aligned} \tan\psi &= \frac{y_e}{x_e}, \\ \tan\omega &= \frac{\sqrt{x_e^2+y_e^2}}{z_e}. \end{aligned} \tag{8}$$

The solutions of this problem become then

$$\begin{aligned} x_{s^{\pm}} &= \cos\omega(S_1^{\pm}\cos\psi + S_3^{\pm}\sin\psi) - S_2^{\pm}\sin\omega, \\ y_{s^{\pm}} &= \sin\omega(S_1^{\pm}\cos\psi + S_3^{\pm}\sin\psi) + S_2^{\pm}\cos\omega, \\ z_{s^{\pm}} &= -S_1^{\pm}\sin\psi + S_3^{\pm}\cos\psi, \end{aligned} \tag{9}$$

where x_s, y_s and the z_s defined component of the two possible directions of the defected ray. One of these lines is directed over the shadow zone and is then not valid. To identify the valid direction, $\vec{u} = \vec{s_-} - \vec{s_+}$ is evaluated and compared to the direction of $\vec{IE}$ which points at the shadow zone. If $\vec{u}\cdot\vec{IE} \geq 0$, the direction $\vec{s}$ is then equal to $\vec{s_+}$ else $\vec{s} = \vec{s_-}$. When the ray is perpendicular to the edge ($\theta = \pi/2$), the diffraction cone becomes a disc and the deflected ray can simply be viewed as rotated around $\vec{e}$ about an angle ϕ.

2.3. Numerical implementation

To detect the possible deflected rays, each diffracting half-plane is topped by a virtual surface, similarly to Refs. [33, 34, 35]. These virtual surfaces are defined by the user and extend the considered half-plane in the same direction. When the surface intersected by a sound ray is a virtual surface, this ray is deflected according to equation (5). There is no splitting up of the ray. The diffraction algorithm can be viewed merely as a kind of specific reflection law. After its deflection, the ray-tracing algorithm is continued as usual [29]. During their travel, the rays can be thus subjected to an unlimited number of reflections or diffractions. Moreover, the reflections can be diffuse or specular and can occur before or after the possible diffractions.

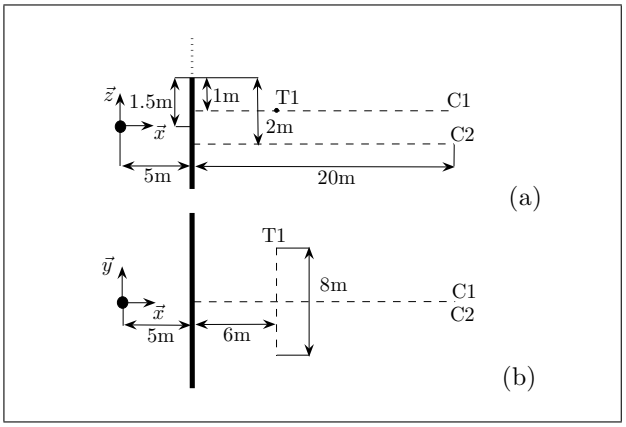

Figure 5. (a) Cross-section of the studied configuration and (b) top-view of the studied configuration. (•) Source location, (dashed line) locations of the sound receivers. The dotted line indicates the location of the virtual surface.

The main cost of the proposed diffraction concept is to add some virtual surfaces that increase the number of tested surfaces during the intersection test. On the other hand, the diffraction model remains independent of the chosen intersection algorithm and benefits of each of its improvement.

The ray-tracing algorithm is known to be prone to sampling issues [42]: the number of emitted rays is limited and some important propagation paths can be missed. The point is even more crucial in the proposed diffraction model. Figure 3 shows that the deflection occurs mainly within the first wavelength over the diffracting edge. So, if the number of rays crossing the detection zone is too low, the shadow zone will be only loosely covered and some discontinuities may appear in the resulting diffracted field as it will be showed in the following section.

3. Numerical validations for a half-plane

In this section, the ray-tracing results are compared with those obtained using the UTD. The studied configuration is a half-plane equivalent to a sound barrier and is presented in Figure 5. The sound source is an omnidirectional point source with a sound power level of 100 dB and three frequencies (125, 500 and 2000 Hz) are considered. The sound pressure level (SPL) is first computed behind the half-plane along two lines following the x axis: the line C1 is located 1m below the diffracting edge and the line C2 2m below (Figure 5a). A third computation line noted down T1 is parallel to the half-plane, following the y axis (Figure 5b). For the ray-tracing simulations, 10^7 rays are emitted. The receivers are spherical with 0.5 m diameter

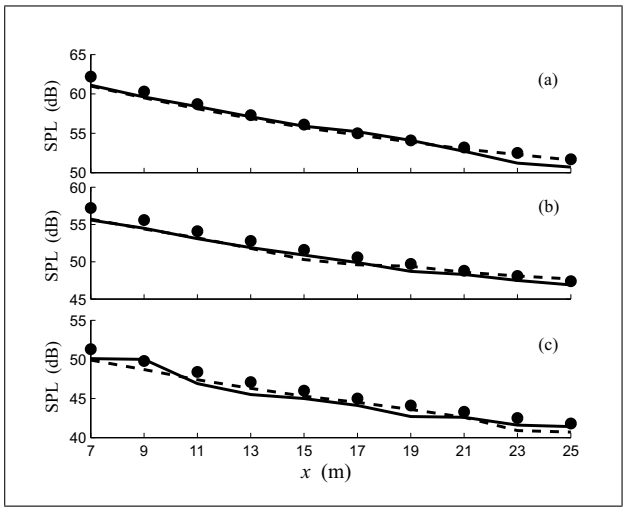

Figure 6. Evolution of the sound pressure level (SPL) along C1 at (a) 125 Hz, (b) 500 Hz and (c) 2000 Hz: (•) uniform theory of diffraction, (thick line) ray-tracing with 10^7 rays and (dashed line) 10^8.

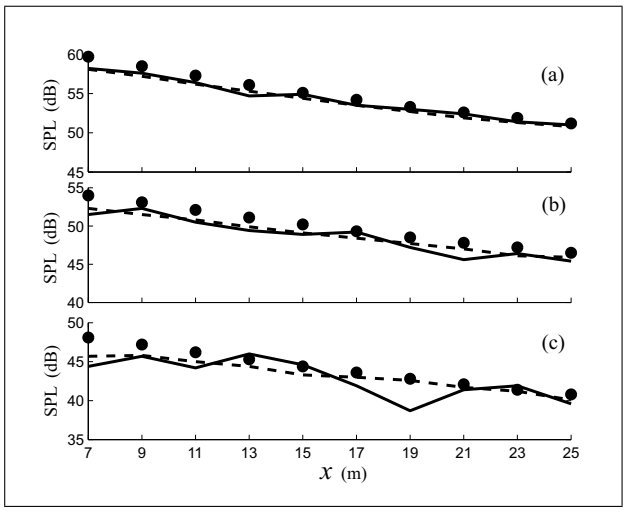

Figure 7. Evolution of the sound pressure level (SPL) along C2 at (a) 125 Hz, (b) 500 Hz and (c) 2000 Hz: (•) uniform theory of diffraction, (thick line) ray-tracing with 10^7 rays and (dashed line) 10^8.

and located every 2 m along C1 and C2 and every meter along T1. This numerical parameters are set arbitrarily to ensure that at least one ray reaches the sound receivers as it will checked in the following. The computation time is about 60 s on a computer fitted with a 2.4 G Hz Pentium 4 with 2 GB of RAM.

The ray tracing's results are in a good agreement with those obtained with the UTD along C1, C2 and T1. The mean discrepancy is less than 2 dB (Figures 6–8). The proposed diffraction model tends to slightly underestimate the sound pressure level compared to the UTD. This underestimation is partly due to the empirical expression of equation (5) and partly to the sampling issue associated with the ray-tracing algorithm. The deviation is thus greater closer to the half-plane and deeper in the shadow zone.

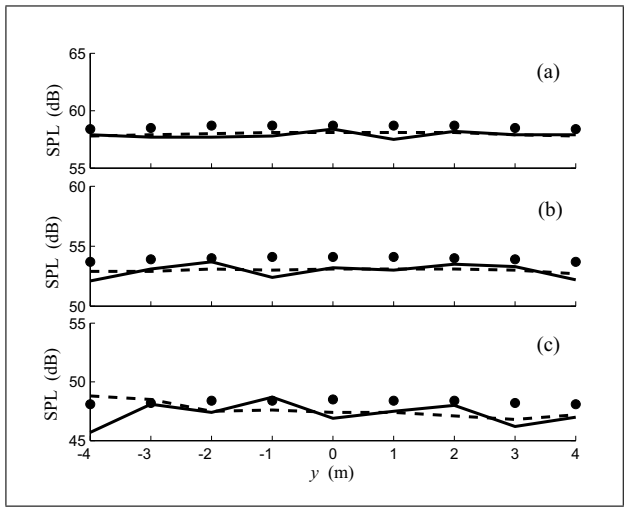

Figure 8. Evolution of the sound pressure level (SPL) along T1 at (a) 125 Hz, (b) 500 Hz and (c) 2000 Hz: (•) uniform theory of diffraction, (thick line) ray-tracing with 10^7 rays and (dashed line) 10^8.

Table I. Mean (Er_m) and maximal (Er_M) discrepancies between the ray-tracing using 10^7 rays and the uniform theory of diffraction results for C1, C2 and T1. All values in dB.

	C1		C2		T1	
Hz	Er_m	Er_M	Er_m	Er_M	Er_m	Er_M
125	0.6	1.3	0.7	1.5	0.7	1.2
500	0.8	1.5	1.3	2.5	1.0	1.7
2000	1.0	1.6	1.6	4.1	0.7	2.4

This corresponds to the greatest deflection angles which are associated with passing distances shorter than 0.1λ (Figure 3). Moreover, both the mean Er_m and the maximal Er_M discrepancies between the ray-tracing and the UTD increase with the frequency (Table I). This is also linked to the decreasing size of the effective surface redirecting the rays with increasing frequency. If this surface is limited to a height equal to 3λ and considering the sound receiver diameter (0.5m), the effective solid angle starting from the source is evaluated to 0.098 Sr at 125 Hz, 0.035 Sr at 500 Hz and 0.009 Sr at 2000 Hz. The number of rays passing through the effective diffracting surface can be then estimated to about 78.10^3 at 125 Hz, 28.10^3 at 500 Hz and 7.10^3 at 2000 Hz. This decreasing number of redirected rays hitting the sound receivers (Figure 9) can explain the under-sampling and the increased errors at high frequencies.

Increasing the number of emitted rays from 10^7 to 10^8 (and similarly increasing the computation time by a factor 10 and is equal to about 600s) has a marginal effect on the results obtained along C1 (Figure 6) at every frequency and along C2 (Figure 7) at 125 Hz (Table II). In this case, the main source of discrepancy is due to the modeling of diffraction. On the other hand, the discrepancies along C2 are effectively reduced at 500 Hz and 2000 Hz and also at 2000 Hz for the results along T1.

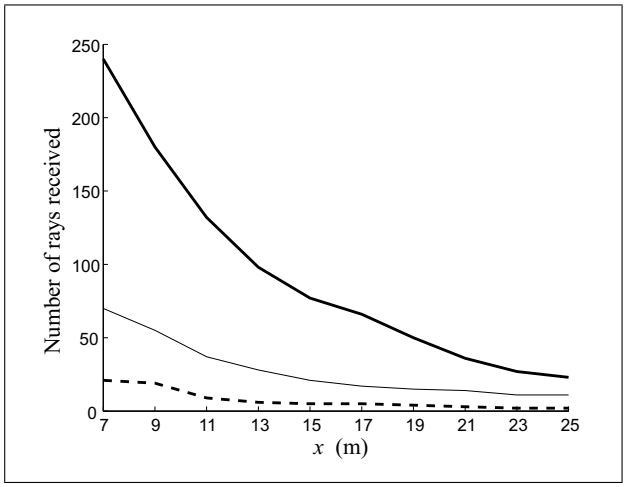

Figure 9. Evolution of the number of rays crossing the spherical sound receivers along the section C2: (thick line) 125 Hz, (thin line) 500 Hz and (dashed line) 2000 Hz.

Table II. Mean (Er_m) and maximal (Er_M) discrepancies between the ray-tracing using 10^8 rays and the uniform theory of diffraction results for C1, C2 and T1. All values in dB.

	C1		C2		T1	
	Er_m	Er_M	Er_m	Er_M	Er_m	Er_M
125	0.4	1.2	0.9	1.6	0.6	0.7
500	0.9	1.6	1.1	1.7	1.0	1.1
2000	0.9	1.6	0.9	2.4	0.9	1.4

4. Computation time

The following test has been carried out to estimate the extra-computing time resulting from the application of the diffraction model in a ray-tracing algorithm. An enclosure is fitted with a varying number of diffracting edges. The sound source is located at one room's corner and a sound receiver at the opposite one. A reference room contains 38 surfaces (without diffracting surface) and is used as a reference simulation. Then, simulations with 1 to 32 additional virtual diffracting surfaces are proceeded. As a comparison, simulations are also performed where the diffracting surfaces are replaced by classical surfaces, without diffraction. The geometrical model comprises then 39 to 70 surfaces. The absorption coefficient is set to 0.1 and the scattering coefficient to 0.5 for all the surfaces. These parameters were arbitrarily set as likely room acoustic parameters and the evaluated additional computation time is weakly affected by these parameters.

The first criterion investigated is ΔT_0 the relative increase of computation time with respect to the reference simulation (38 surfaces without diffraction, Figure 10a). The computation time with the diffraction model increases linearly with the number of surfaces, as it is usual with ray-tracing algorithms. Compared to the configurations without diffraction model, the computation time increase ΔT_0 is about 50% with the diffraction model.

The simulations with and without diffraction can also be compared for the same number of surfaces through the criterion ΔT_1 (Figure 10b). The increase of computation time can roughly be estimated to around 1% when one classical surface is replaced by a diffracting surface. However, it should pointed out that higher number of rays must be emitted to keep the accuracy of the results at a reasonable level.

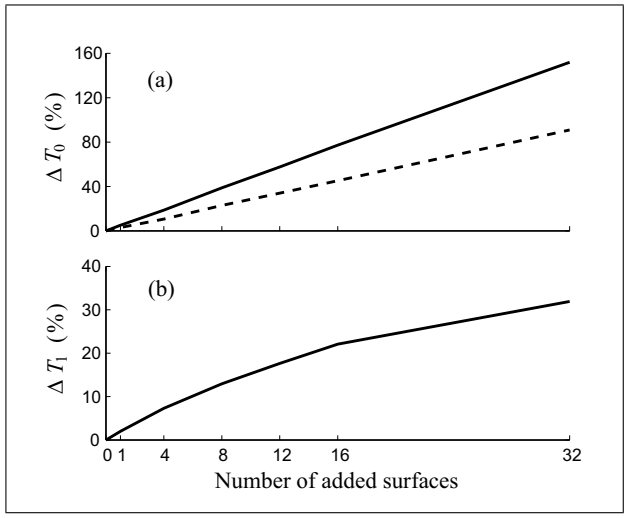

Figure 10. Evolution of the computation time as a function of the number of added surfaces. (a) ΔT_0 is evaluated in respect to the reference simulation with 38 surfaces: (thick line) the added surfaces are diffracting and (dashed line) the added surfaces are not diffracting. (b) ΔT_1 compares the simulations with diffraction to the ones without diffraction for the same number of surfaces.

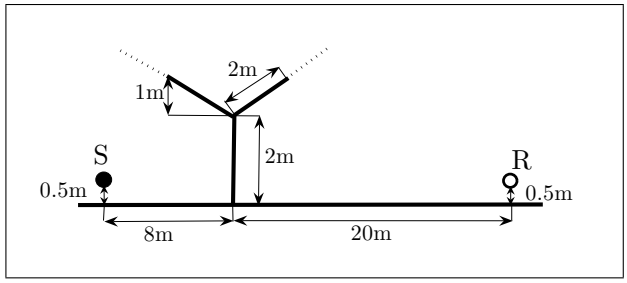

Figure 11. Sketch of the simulated Y-shaped barrier. S indicates the sound source location and R the sound receiver. The dotted lines indicate the locations of the virtual surfaces.

5. Application to a Y-shaped sound barrier

In this section, an application to a double diffraction problem is presented. A Y-shaped barrier (Figure 11) is considered and comparison with numerical data obtained with the boundary element method [43] is carried out for the frequency range from 100 Hz to 1000 Hz. The ground and the barrier are assumed perfectly rigid (without scattering and absorption). For the ray-tracing simulations, 10^7 rays are emitted and the sound receiver is a 0.5m diameter sphere. In this configuration, there are two virtual surfaces that extend each branch of the barrier.

Despite neglecting the interference effects, the ray-tracing is globally in good agreement with the reference

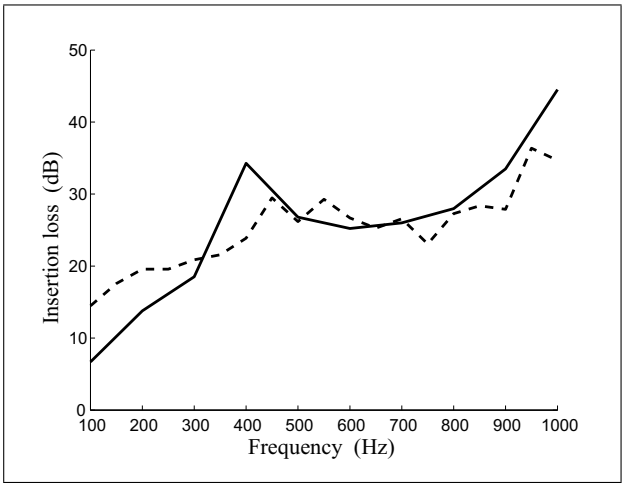

Figure 12. Insertion loss at the receiver as a function of the frequency: (thick line) numerical data [43], (dashed line) ray-tracing results.

data (Figure 12). It tends to overestimate the insertion loss below 300 Hz and cannot predict an insertion loss peak occurring at 400 Hz. In fact, this peak must be due to interference effects which are not taken into account by the proposed model. On the other hand, the agreement is very good above 500 Hz.

6. Conclusion

The ray-tracing method is a geometrical acoustics model approximating the propagation of sound waves by rays carrying only energy information. This obtained mode is very popular in room acoustics and auralization due to its low computation load. However, diffraction effects is seldom modeled, restricting its application.

In this paper, a diffraction model developed to predict the scattering of light by ice crystals is adapted to an acoustic ray-tracing software. To simulate diffraction by half-planes, the rays passing in the vicinity of the diffracting edges are deflected in the shadow zone depending on the ray-edge distance and on the frequency. The deflection law is based on an approximation of the far field direction of the time-averaged Poynting's vector. This model assumes that the edge is infinite and that the source and the receiver are far enough from the diffracting edge. This model is here extended to obliquely incident rays and compared to the uniform theory of diffraction for a half-plane.

The obtained results agree well for the tested configurations, with mean discrepancies lower than 2 dB. These discrepancies are due to the approximated deflection law, on the one hand, and to sampling issues, on the other hand. In fact, the deflection of the rays occurs mainly within the first wavelength over the half-plane. In this deflecting zone, the number of rays must be great enough to completely cover the shadow zone, without discontinuities. So, the obtained predictions are more reliable at lower frequencies for a given number of rays.

In addition, a configuration composed of a Y-shaped barrier on a rigid flat ground was also investigated, this geometry presenting a double diffraction phenomenon. Despite neglecting the interference effects, a fair agreement is found between ray-tracing and boundary elements method results for frequencies ranging between 100 Hz and 1000 Hz.

Concerning the computation time, the proposed model shows to be very efficient. The computation time grows linearly with the number of diffracting edges and increases by an amount of 1% by added diffracting edge compared to classical non-diffracting surfaces. Moreover, the proposed model is only a variation of the ray-tracing algorithm and it is therefore compatible with most of ray-tracing accelerating techniques.

Further work must be done to improve the presented diffraction algorithm and extend it to deal with wedges of arbitrary angle and slits.

Acknowledgments

Alexis Billon wishes to thank the *Fonds de la Recherche Scientifique* (Belgian National Fund for Scientific Research FNRS) for providing financial support to this work (Grant 2.4.534.09.F).

References

[1] H. Kuttruff: Room acoustics. 4th ed. Taylor & Francis, London, 2000.

[2] J.-D. Polack: Modifying chambers to play billiards: the foundation of reverberation theory. Acustica **76** (1992) 257–272.

[3] M. Kleiner, B.-I. Dalenbäck, U. Svensson: Auralization – an overview. J. Audio Eng. Soc. **41** (1993) 861–875.

[4] M. Vorländer: Auralization. Springer, Berlin, 2007.

[5] I. Bork: A comparison of room simulation software - the 2nd round robin on room acoustical computer simulation. Acustica united with Acta Acustica **86** (2000) 943–956.

[6] R. Torres, U. Svensson, M. Kleiner: Computation of edge diffraction for more accurate room acoustics auralization. J. Acoust. Soc. Am. **109** (2001) 600–610.

[7] G. Kouyoumjian, P. Pathak: A uniform geometrical theory of diffraction for an edge in a perfectly conducting surface. Proc. IEEE **62** (1974) 1448–1461.

[8] D. McNamara, C. Pistorius, J. Malherbe: Introduction to the uniform geometrical theory of diffraction. Artec House, Boston, 1990.

[9] M. Biot, I. Tolstoy: Formulation of wave propagation in infinite media by normal coordinates with an application to diffraction. J. Acoust. Soc. Am. **29** (1957) 381–391.

[10] H. Medwin: Shadowing by finite noise barriers. J. Acoust. Soc. Am. **69** (1981) 1060–1064.

[11] U. Svensson, R. Fred, J. Vanderkooy: An analytic secondary source model of edge diffraction impulse responses. J. Acoust. Soc. Am. **106** (1999) 2331–2344.

[12] N. Tsingos, T. Funkhouser, A. Ngan, I. Carlbom: Modeling acoustics in virtual environments using the uniform theory of diffraction. Proc. ACM Computer Graphics (SIGGRAPH–01), 2001, 545–552.

[13] T. Funkhouser, N. Tsingos, I. Carlbom, G. Elko, J. West, G. Pingali, P. Min, A. Ngan: A beam tracing method for

interactive architectural acoustics. J. Acoust. Soc. Am. **115** (2004) 739–756.

[14] A. Chandak, C. Lauterbach, M. Taylor, Z. Ren, D. Manocha: Adfrustum: Adaptive frustum tracing for interactive sound propagation. IEEE T. Vis. Comput. Gr. **14** (2008) 1707–1722.

[15] M. Taylor, A. Chandak, Z. Ren, C. Lauterbach, D. Manocha: Fast edge-diffraction for sound propagation in complex virtual environments. Proc. EAA Symposium on Auralization, 2009, 1–6.

[16] V. Pulkki, T. Lokk, L. Savojia: Implementation and visualization of edge diffraction with image-source method. 112th AES Convention, 2002, Preprint 5603.

[17] D. Schröder, A. Pohl: Real-time hybrid simulation method including edge. Proc. EAA Symposium on Auralization, 2009, 1–6.

[18] P. Calamia, U. Svensson: Fast time-domain edge-diffraction calculations for interactive acoustic simulations. EURASIP J. Adv. Sig. Pr. (2007) 1–10.

[19] P. Calamia, B. Markham, U. Svensson: Diffraction culling for virtual-acoustic simulations. Acta Acustica united with Acustica **94** (2008) 907–920.

[20] U. Svensson, P. Calamia, S. Nakanishi: Frequency-domain edge diffraction for finite and infinite edges. Acta Acustica united with Acustica **95** (2009) 568–572.

[21] A. Asheim, U. Svensson: Efficient evaluation of edge diffraction integrals using the numerical method of steepest descent. J. Acoust. Soc. Am. **128** (2010) 1590–1597.

[22] D. Ouis: Noise attenuation by a hard wedge-shaped barrier. J. Sound Vib. **262** (2003) 347–364.

[23] D. Ouis: Scattering by a barrier in a room. Appl. Acoust. **56** (1999) 1–24.

[24] J. Allen, D. Berkley: Image method for efficiently simulating small-room acoustics. J. Acoust. Soc. Am. **65** (1979) 943–950.

[25] J. Borish: Extension of the image model to arbitrary polyhedra. J. Acoust. Soc. Am. **75** (1984) 1827–1836.

[26] D. Schröder, T. Lentz: Real-time processing of image sources using binary space partitioning. J. Audio Eng. Soc. **54** (2007) 604–619.

[27] A. Farina: Validation of the pyramid tracing algorithm for sound propagation outdoors: comparison with experimental measurements and with the ISO–DIS 9613 standards. Adv. Eng. Softw. **31** (2000) 241–250.

[28] A. Krokstad, S. Strom, S. Sorsdal: Calculating the acoustical room response by the use of a ray tracing technique. J. Sound Vib. **8** (1968) 118–125.

[29] A. Kulowski: Algorithmic representation of the ray tracing technique. Appl. Acoust. **18** (1985) 449–469.

[30] M. Hodgson: Evidence of diffuse surface reflections in rooms. J. Acoust. Soc. Am. **89** (1991) 765–771.

[31] J.-J. Embrechts: Broad spectrum diffusion model for room acoustics ray-tracing algorithms. J. Acoust. Soc. Am. **107** (2000) 2068–2081.

[32] S. Dance, B. Shield: Modelling of sound fields in enclosed spaces with absorbent room surfaces. Part III: Barriers. Appl. Acoust. **61** (2000) 385–397.

[33] G. Benedetto, R. Spagnolo: A study of barriers in enclosures by a ray-tracing computer model. Appl. Acoust. **17** (1984) 183–199.

[34] U. Stephenson: An energetic approach for the simulation of diffraction with ray tracing based on the uncertainty relation. Acta Acustica united with Acustica **96** (2010) 516–535.

[35] U. Stephenson: An analytically derived sound particle diffraction model. Acta Acustica united with Acustica **96** (2010) 1051–1068.

[36] J. Keller: Geometrical theory of diffraction. J. Opt. Soc. Am. **52** (1962) 116–130.

[37] E. Hesse, Z. Ulanowski: Scattering from long prisms computed using ray tracing combined with diffraction facets. J. Quant. Spectrosc. Ra. **79-80** (2003) 721–732.

[38] M. Born, E. Wolf: Principles of optics. 3rd ed.,. Pergamon Press, New York, 1965.

[39] A. Sommerfeld: Optics. Lecture on theoretical physics: IV. Academic Press, New York, 1964.

[40] A. Pierce: Acoustics: An introduction to its physical principles and applications. Acoustical Society of America, Woodbury, 1989.

[41] E. Hesse: Modelling diffraction during ray tracing using the concept of energy flow lines. J. Quant. Spectrosc. Ra. **109** (2008) 1374–1383.

[42] H. Lehnert: Systematic errors of ray-tracing algorithm. Appl. Acoust. **38** (1993) 207–221.

[43] H. Kim, J. Kim, H. Kang, B. Kim, S. Kim: Sound diffraction by multiple wedges and thin screens. Appl. Acoust. **66** (2005) 1102–1119.